OPEN ACCESS

REPORT

The Innovation Energy

# Day-Night energy harvesting: Photovoltaics-driven moisture evaporation and absorption for simultaneous 24-hour power and dehumidification

Lei Che,[1,5] Niansi Li,[1,5] Wei Wei,[1,5] Jing Li,[1] Jie Ji,[2] Xudong Zhao,[3] Bendong Yu,[1,*] and Qiliang Wang[4,*]

*Correspondence: bendongyu@njtech.edu.cn (B. Y.); qiliang.wang@ustc.edu (Q. W.)

Received: January 4, 2025; Accepted: March 4, 2025; Published Online: April 11, 2025; https://doi.org/10.59717/j.xinn-energy.2025.100078



## GRAPHICAL ABSTRACT

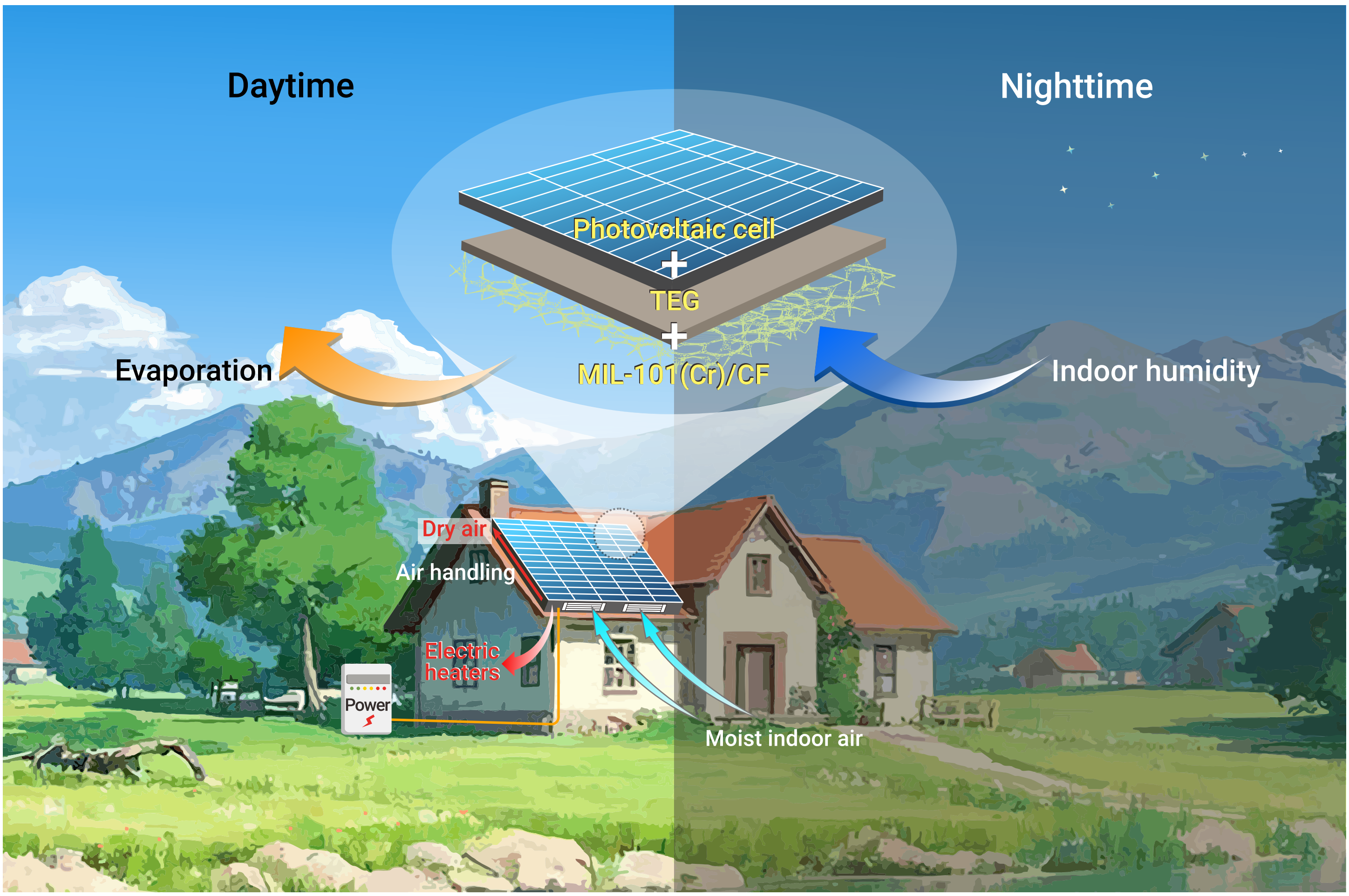


## PUBLIC SUMMARY

- Hybrid system enhances PV efficiency by 23% and thermoelectric efficiency by 353%.
- Reduces relative humidity from 79.12% to 63.34% in 4 hours.
- Generates $1.08\times10^4$ to $1.69\times10^4$ kW annually, saving up to 498 kW in air-conditioning energy.

# Day-Night energy harvesting: Photovoltaics-driven moisture evaporation and absorption for simultaneous 24-hour power and dehumidification

**Lei Che,[1,5] Niansi Li,[1,5] Wei Wei,[1,5] Jing Li,[1] Jie Ji,[2] Xudong Zhao,[3] Bendong Yu,[1,*] and Qiliang Wang[4,*]**

[1]College of Urban Construction, Nanjing Tech University, Nanjing 210009, China

[2]Department of Thermal Science and Energy Engineering, University of Science and Technology of China, Hefei 230026, China

[3]Centre for Sustainable Energy Technologies, University of Hull, Hull HU6 7RX, United Kingdom

[4]Department of Architecture and Built Environment, University of Nottingham, Nottingham NG7 2RD, United Kingdom

[5]These authors contributed equally

*Correspondence: bendongyu@njtech.edu.cn (B. Y.); qiliang.wang@ustc.edu (Q. W.)

Received: January 4, 2025; Accepted: March 4, 2025; Published Online: April 11, 2025; https://doi.org/10.59717/j.xinn-energy.2025.100078



Citation: Che L., Li N., Wei W., et al. (2025). Day-Night energy harvesting: Photovoltaics-driven moisture evaporation and absorption for simultaneous 24-hour power and dehumidification. *The Innovation Energy* **2**:100078.

Building sector is a significant contributor to global carbon emission, primarily driven by electricity consumption and air-conditioning demands. A sustainable pathway toward building decarbonization involves harnessing solar energy to simultaneously generate electricity and address indoor humidity control. In this work, we present an innovative hybrid system that integrates photovoltaic cells, thermoelectric generators, and metal-organic frameworks to enable all-day power generation and efficient air dehumidification. This system leverages the synergy between moisture-induced adsorption/desorption heat from MOFs and the harvesting of solar heat and radiative cooling from PV cells. Notably, the synergistic effects significantly enhanced the PV efficiency of the photovoltaic cell by 23% due to the intensified heat exchange during moisture desorption, and increased the average thermoelectric efficiency by 353%. Additionally, it effectively reduced the air relative humidity from an average of 79.12% to 63.34% within 4 hours. We further demonstrate the application of this hybrid system on building roofs, achieving maximum power densities of 88 $W \cdot m^{-2}$ during the day and 2.12 $W \cdot m^{-2}$ at night in Nanjing, respectively. Across various cities in China, the system shows the annual power generated ranges from $1.08\times10^4$ to $1.69\times10^4$ kW, along with air-conditioning energy savings between 29 and 498 kW. This novel approach provides a low-energy and sustainable solution for continuous power generation and air dehumidification, supporting the decarbonization of buildings.

## INTRODUCTION

Global building energy consumption accounts for about one-third of global energy consumption and also for about one-quarter of global carbon emissions,[1,2] making it a critical area for reducing overall emissions. Building energy demand is mainly driven by the electricity usage, powering systems such as air-conditioning systems, lighting and various appliances.[3] Among these, air-conditioning systems, which provide cooling and dehumidification, are particularly energy-intensive, making them a significant target for efficiency improvements. Given the escalating need for indoor comfort in an urbanizing world, solutions to reduce energy consumption in buildings are of great importance.

Humidity control in buildings plays a vital role in maintaining indoor air quality and human comfort. Conventional air conditioning systems achieve dehumidification by cooling air to its dew point, condensing the moisture, and subsequently removing it, a process that which consumes substantial amounts of energy.[4,5] Indeed, humidity control alone accounts for about 30% of building energy consumption for air-conditioning systems.[6] To reduce the energy consumption of indoors humidity control, various new ideas for dehumidification technologies for buildings have recently emerged,[7-10] such as solid dehumidification, liquid dehumidification and membrane dehumidification. Among these, solid dehumidification, particularly using materials like metal-organic frameworks (MOFs), has emerged as an attractive solution due to its environmental benefits and high performance. MOFs, such as MIL-101 (Cr),[11-13] MOF-801,[14,15] MIL-100 (Fe)[16] are notable for their high specific surface area, adjustable pore size, and excellent moisture-absorbing properties. However, a key challenge with MOF-based solid dehumidification lies in the energy-intensive process of regenerating these materials following moisture adsorption.

On the other hand, photovoltaic cells offer a promising approach for reducing building energy consumption by converting solar energy into electricity.[17,18] By 2030, global PV capacity is expected to exceed 3,500 $GW_p$, with projections indicating over 15,000 $GW_p$ by 2050.[19] Buildings present an ideal platform for integrating PV systems through Building Integrated Photovoltaics (BIPV), such as photovoltaic curtain walls,[19-21] photovoltaic windows,[22-24] photovoltaic roofs,[25-28] which can provide electricity, hot water, heating and ventilation to buildings without changing the original configuration of the borrowed building. Despite their benefits, PV systems generate excess heat during operation, which reduces their efficiency (typically by 0.4%-0.5% per °C).[29-32] Thermoelectric generator (TEG) technology can convert thermal energy into electricity through the Seebeck effect[33,34] (Table S1). By utilizing TEG systems to recover waste heat from PV systems and transform it into supplementary electrical power, this integrated approach effectively enhances the overall photoelectric conversion efficiency of the system.

In this context, we propose an innovative PV-TEG-MOF hybrid system to address both the dehumidification challenge and the efficiency limitations of PV systems. This multifunctional device combines photovoltaics with thermoelectric generators (TEGs) and MOF-based solid dehumidification materials. During the day, solar energy powers the system, enabling simultaneous electricity generation from both PV and TEG modules. As the adsorbed moisture in the MOF material undergoes desorption, the heat absorbed by the MOF reduces the temperature on the cold side of the TEG, enhancing its power density. Additionally, the TEG module extracts excess heat from the PV modules, improving their electrical efficiency and contributing to the overall system's synergistic power generation. At night, the system leverages radiative cooling and the moisture adsorption process of the MOF materials to achieve both dehumidification and power generation. The MOF efficiently captures moisture from the air, releasing adsorption heat, which raises the temperature on the hot side of the TEG. Simultaneously, the radiative cooling effect from the PV module generates cold energy, creating a temperature gradient that further enhances the thermoelectric power output and improves the dehumidification efficiency.

Applied to building roofs across various cities in China, this PV-TEG-MOF hybrid device has demonstrated substantial benefits in terms of energy savings and power generation. Annual power production from the system ranges between $1.08 \times 10^4$ kW and $1.69 \times 10^4$ kW, while air-conditioning energy savings range from 29 kW to 498 kW per year. This work presents a novel route to achieving efficient, all-day dehumidification and power generation, ultimately contributing to reduced energy demand in buildings and improved indoor comfort.

## MATERIALS AND METHODS

### Preparation of MIL-101(Cr)/CF composite

Chromic chloride hexahydrate ($CrCl_3 \cdot 6H_2O$), terephthalic acid ($C_6H_4$–1,4-$(CO_2H)_2$), N, N-Dimethyl formamide (DMF), ethanol, and all raw Chemicals were purchased from Sigma-Aldrich. Firstly, MIL-101(Cr) was synthesized using a hydrothermal reaction. 7 mmol chromic chloride hexahydrate and 7 mmol terephthalic acid were dissolved into 50.4 mL deionized water. The mixed solution was magnetically mixed at room temperature for 30 minutes, then loaded into a hydrothermal reaction (100 mL), and then subjected to hydrothermal treatment at 190 °C for 24 hours. The MIL-101(Cr) product was then collected by centrifugation and washed with DMF, ethanol and deionized water. Secondly, the MIL-101(Cr) suspension was prepared by mixing 3 g MIL-101(Cr) powder with 24 mL ethanol and 6 mL water, and then 0.3 g of sodium silicate (~10wt%) was added to the suspension as binder. The synthesized MOF suspension was filled into the open pores of the CF and then dried at 105 °C for 24 h to form a robust MOF coating on the skeleton of the porous CF.

### Characterizations of MIL-101(Cr)/CF composite

The powder X-ray diffraction pattern of MIL-101(Cr)/CF was measured using a multi-functional X-ray powder diffractometer (D8 Advance Da Vinci, Bruker) in the 2θ range of 5–30°. The morphology was observed using Scanning Electron Microscopy (SEM, Gemini sigma 300, Zeiss). The nitrogen adsorption was measured using physisorption apparatus (ASAP 2460, Micromeritics) and the specific surface area is determined by Brunauer-Emmett-Teller (BET) method. The water vapor sorption isotherms were measured using an SMS-DVS Intrisic.

### Water uptake of MIL-101(Cr)/CF composite

The water uptake of MIL-101(Cr)/CF was measured using a self-constructed adsorption test device with a precision electronic balance (Note S1). Before each test, the composite samples were dried at 60 °C for 4 h. Then, the samples were sealed and cooled to room temperature and placed on an electronic balance under predetermined ambient conditions. The mass change of the samples during water vapor adsorption was continuously recorded until their adsorption equilibrium was reached. The water absorption ($g_{water} \cdot g_{adsorbent}^{-1}$) of was calculated from the mass difference of the composites before and after water adsorption.

### Performance of hybrid PV-TEG-MOF device

Indoor and outdoor experiments were carried out to evaluate the performance of hybrid PV-TEG-MOF device. For the indoor experiments, all proof-of-concept experiments for the hybrid device were conducted at controlled temperatures and relative humidities, with fluctuations in temperature and relative humidity kept below 1°C and 3%, as measured by a temperature sensor (K-Type Thermocouple) and humidity sensor (KS-SH51AP). Indoor simulated nighttime experiments used water-cooled panels to simulate radiative cooling to accelerate the hygroscopicity of the hybrid device at 25 °C and 80% RH. Indoor simulated daytime experiments were conducted at light intensities of 600, 800 and 1000 $W \cdot m^{-2}$ using a sunlight simulator for moisture desorption with a uniformity of 10%, a temporal instability of 10% and a spectral match classification of AAA. For the outdoor experiments, the hybrid device was placed on the roof of our Tiangong Building at Nanjing Tech University, and a transparent polyethylene membrane was used to suppress convective heat loss from the hybrid device. At night, moisture adsorption occurred from 00:00 AM to 04:00 AM (UTC+8), and radiative cooling enhanced moisture adsorption and power generation. During the day, moisture desorption occurs by driving the hybrid device between 12:00 PM and 15:00 PM (UTC + 8). The solar flux was measured in real time by a solar intensity meter. As a contrast, a reference device without MOF adsorbent was prepared and tested to evaluate the effect of moisture adsorption/desorption on power generation performance. Changes in temperature and relative humidity were measured in real time by installing temperature and relative humidity sensors inside the hybrid device.

### Thermal and electrical transfer model of hybrid device

We obtained the typical meteorological year data for 34 provincial capital cities from *EnergyPlus* software, including basic weather parameters such as temperature, humidity, and wind speed. These data were used as model inputs, enabling us to accurately simulate the system's performance under different climatic conditions. We then input these parameters into *MATLAB* and performed iterative calculations to simulate the system's energy efficiency, dehumidification, and energy-saving effects under various operating modes (Figure S21). Ultimately, these simulation results provided strong data support for evaluating the performance of the PV-TEG-MOF system under different climate conditions throughout the year.

In the numerical model, $T_p$, $T_a$, and $T_{mof}$ (°C) were the temperatures of the PV cell, moist air airflow and MOF material, respectively.

The energy balance function for the glass cover was given as:

$$\rho_g \delta_g c_g \frac{\partial T_g}{\partial t} = G_g + h_{c\_adm}(T_{adm} - T_g) + h_{r\_skv}(T_{sky} - T_g) + h_{r\_sp}(T_p - T_g) + \frac{k_g}{\delta_g}(T_p - T_g) \quad (1)$$

where $\rho_g$ was density of glass cover ($kg \cdot m^{-3}$); $\delta_g$ was thickness of the glass cover (m); $c_g$ was the capacity of the glass cover ($J \cdot K^{-1} \cdot m^{-2}$); $G_g$ was the solar radiation intensity on the surface of glass cover ($W \cdot m^{-2}$); $h_{c\_abm}$ was convective heat transfer coefficient between glass cover and ambient air ($W \cdot m^{-2} \cdot K^{-1}$) ; $h_{r\_sky}$ was sky temperature radiation coefficient ($W \cdot m^{-2} \cdot K^{-1}$), radiant heat transfer depended on the Stefan-Boltzmann law, and could be calculated via the emissivity of the object;[35] $h_{r\_gp}$ was the radiant heat transfer coefficient between the glass cover and PV cell ($W \cdot m^{-2} \cdot K^{-1}$) ; $k_g$ was thermal conductivity of glass cover ($W \cdot m^{-2} \cdot K^{-1}$).The irradiation intensity at different angles could refer to the Spencer model. The calculation formula of the irradiation intensity of the model was as flowed:

$$G_g = \int_{300}^{4000} \alpha_g(\lambda) G(\lambda) d\lambda \sin(h) \cos(\beta) \quad (2)$$

$$\sin(h) = \sin\phi \sin\delta + \cos\phi \cos\delta \cos h_a \quad (3)$$

$$h_{r\_sky} = \sigma \varepsilon_g (T_{sky} + T_g)(T_{sky}^2 + T_g^2) \quad (4)$$

$$T_{sky} = 0.0552 T_a^{1.15} \quad (5)$$

$$h_{c\_abm} = 6.5 + 3.3 u_a \quad (6)$$

$$h_{r\_gp} = \frac{\sigma (T_p + T_g)(T_p^2 + T_g^2)}{1/\varepsilon_g + 1/\varepsilon_p} \quad (7)$$

The energy balance function for the PV cell was given as:

$$\rho_p \delta_p c_p \frac{\partial T_p}{\partial t} = G_p - Q_e + h_{c\_abm}(T_{abm} - T_p) + h_{r\_gp}(T_g - T_p) + h_{r\_preg}(T_{teg} - T_p) + \frac{k_p}{\delta_p}(T_g - T_p) + \frac{k_p}{\delta_p}(T_{teg} - T_p) \quad (8)$$

where $\rho_p$ was density of PV cell ($kg \cdot m^{-3}$); $\delta_p$ was thickness of the PV cell (m); $c_p$ was the capacity of the PV cell ($J \cdot K^{-1} \cdot m^{-2}$); $G_p$ was the solar radiation intensity on the surface of PV cell ($W \cdot m^{-2}$); $Qe$ was the output power of PV cell; $h_{r\_pteg}$ was the radiant heat transfer coefficient between the PV cell and TEG panel ($W \cdot m^{-2} \cdot K^{-1}$); $k_p$ was thermal conductivity of PV cell ($W \cdot m^{-2} \cdot K^{-1}$).

$$G_p = \int_{300}^{4000} \tau_g(\lambda) \alpha_p(\lambda) G(\lambda) d\lambda \sin(h) \cos(\beta) \quad (9)$$

$$h_{r\_pteg} = \frac{\sigma (T_p + T_{teg})(T_p^2 + T_{teg}^2)}{1/\varepsilon_p + 1/\varepsilon_{teg}} \quad (10)$$

The energy balance function for the TEG panel was given as:

$$\rho_{teg} \delta_{teg} c_{teg} \frac{\partial T_{teg}}{\partial t} = \frac{k_{teg}}{\delta_{teg}}(T_p - T_{teg}) + \frac{k_{teg}}{\delta_{teg}}(T_{mof} - T_{teg}) \quad (11)$$

where $\rho_{teg}$ was density of TEG panel ($kg \cdot m^{-3}$); $\delta_{teg}$ was thickness of the TEG panel (m); $c_{teg}$ was the capacity of the TEG panel ($J \cdot K^{-1} \cdot m^{-2}$); $k_{teg}$ was thermal conductivity of TEG panel ($W \cdot m^{-2} \cdot K^{-1}$).

The following equation is the heat and mass transfer equation of MOF:

$$\rho_d c_{tot} \frac{\partial T_{mof}}{\partial t} = k_d \left( \frac{\partial T_{mof}}{\partial x} + \frac{\partial T_{mof}}{\partial y} \right) + q_{st} \rho_d \frac{\delta w}{\delta t} \quad (12)$$

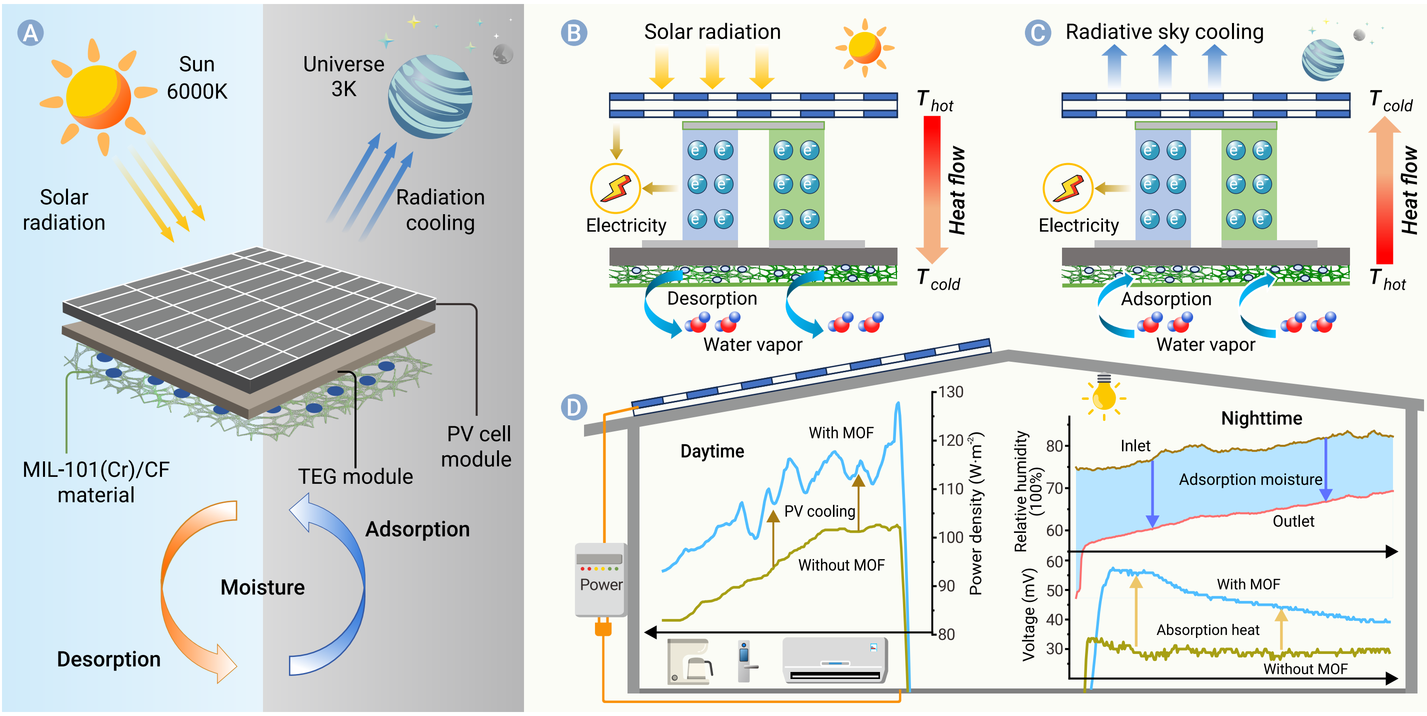


**Figure 1. All-day power generation and dehumidification principle** a Schematic diagram of the structure and all-day operation of hybrid PV-TEG-MOF device. b Energy balance of hybrid PV-TEG-MOF by radiative heating during daytime. c Energy balance of hybrid PV-TEG-MOF by radiative cooling and moisture-desorption during nighttime. d Building roof application and performance of PV-TEG-MOF device.

where $\rho_d$ was density of dry absorbent (kg·m$^{-3}$); $k_d$ was thermal conductivity of dry absorbent (W·(m·K)$^{-1}$); $w$ was moisture content of hygroscopic agent (kg·kg$^{-1}$); $q_{st}$ was adsorption heat (kJ·kg$^{-1}$); $c_{tot}$ was the total heat capacity of MOF materials (kJ·kg$^{-1}$).

$$c_{tot} = c_{pd} + wc_{pw} \tag{13}$$

$$w = \frac{f_d W_{max}}{1 - C + C/RH} \tag{14}$$

where $W_{max}$ was maximum adsorption capacity (kg·kg$^{-1}$); $C$ was a constant, which determined the shape of the adsorption isotherm. RH was relative humidity; $f_d$ was mass ratio of effective adsorbent.

The heat and mass transfer equation of airflow can be calculated according to the following formulas:

$$\frac{1}{u_m}\frac{\partial T_a}{\partial t} + \frac{\partial T_a}{\partial y} = \frac{4h}{d_e u_m \rho_a c_a}(T_{mof} - T_a) \tag{15}$$

$$\frac{1}{u_m}\frac{\partial (d_a)}{\partial t} + \frac{\partial (d_a)}{\partial y} = \frac{4h_m}{d_e u_m}(d_{mof} - d_a) \tag{16}$$

where $\rho_a$ was density of moist air (kg·m$^{-3}$); $c_a$ was the capacity of moist air (J·K$^{-1}$·m$^{-2}$); $u_m$ was the average velocity of the airflow (m·s$^{-1}$); $d_a$ was moisture content of airflow (g·kg$^{-1}$); $d_{mof}$ was moisture content of MOF (g·kg$^{-1}$); $d_e$ was flux equivalent diameter (m); $y$ was axial coordinates along the flow channel direction (m); $h$ was convective heat transfer coefficient between moist air and MOF; $h_m$ was convective mass transfer coefficient between moist air and MOF; Le$^{2/3}$ was the Lewis number.

$$h_m = \frac{h}{\rho_a c_a Le^{2/3}} \tag{17}$$

The power generation of PV cells refers to the instantaneous electric energy generated by PV cells, which can be calculated by the following expression:[36]

$$E_{pv} = G\tau_g \zeta \eta_{ref}[1 - B_r(T_{pv} - T_{ref})] \tag{18}$$

where, $E_{pv}$ is the electrical power output of PV cells, with the units of W·m$^{-2}$, $\xi$ is the $T_{ref}$ is the reference temperature, $\eta_{ref}$ is the standard PV efficiency under the reference temperature (25 °C) and $B_r$ is the temperature coefficient.

## RESULTS

### Principle of all-day electric power generation and humidity control

Herein, we propose an all-day power generation and simultaneous air dehumidification device enabled by energy harvesting from sun and space by PV cells. The hybrid PV-TEG-MOF device mainly consists of PV module, TEG module and MOF module, respectively (Figure 1). The PV modules, TEG modules and MOF modules arranged from top to bottom, and each module uses a thermally conductive adhesive to reduce the thermal resistance between them. The PV generates electricity during the daytime, while the TEG can utilize the temperature difference between the PV module and the MOF module to generate electricity throughout the day. The adsorbent for MOF module can achieve indoor dehumidification at nighttime and realize regeneration by using the waste heat of photovoltaics during the daytime (Figure 1D). The electricity generated by the hybrid device during the daytime and nighttime can be stored to power indoor appliances, such as air conditioner, mobile phone charging and lighting (Figure S1). Besides, the power generated also can be supplied to an electric auxiliary heat module for MOF desorption in areas with insufficient sunlight or low temperatures.

During daytime (Figure 1B), the PV cell is used as the solar radiation absorbing part of the hybrid device, which can effectively capture solar radiation for power and thermal energy co-generation due to its high solar absorptivity (Figure S6d). The waste heat released from the PV module is transmitted to TEG and MOF module through heat conduction. The saturated solid dehumidification material, which completes the dehumidification process during the night, absorbs heat to complete the regeneration process driven by heat, forming the cold end of the TEG module. In conventional TEG system design, the cold end is created by air-cooling, water-cooling.[37,44] However, we generated the cold end by desorbing heat from the MOF for efficient cooling without the need for an additional device. Because moisture desorption can remove a large amount of photovoltaic heat during the desorption process, thereby lowering the temperature at the cold end of the TEG and driving the PV-TEG to achieve better electric conversion (Figure 1D). The temperature difference between the hot end (PV side) and the cold end (MOF side) of the thermoelectric module generated power through the Seebeck effect.[38]

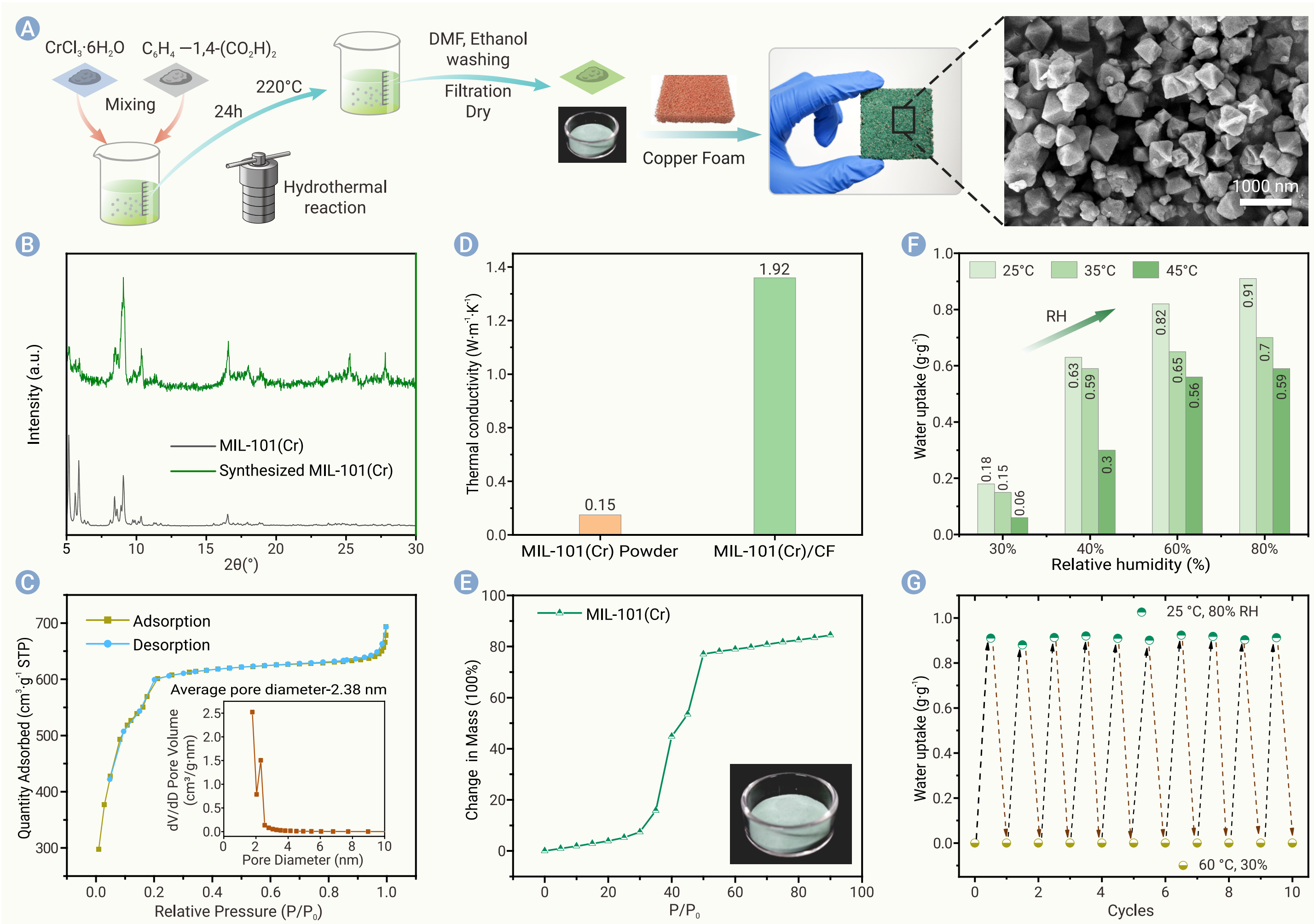


**Figure 2. Synthesis and characterization of MIL-101(Cr)/CF composite for water sorption** a Synthesis procedure and SEM images of MIL-101(Cr)/CF composite (size: 50×50×5 mm). b XRD patterns of MIL-101(Cr). c Nitrogen adsorption-desorption isotherms of MIL-101(Cr). d Thermal conductivities of MIL-101(Cr) powder and MIL-101(Cr)/CF composite. e Water adsorption isotherms of MIL-101(Cr) with typical S-shaped characteristics and high-water uptake at 25 °C. f Water uptake of MIL-101(Cr)/CF composite samples at different temperature and RH. g Cycling stability of moisture absorption-desorption of MIL-101(Cr)/CF (absorption at 25 °C and 80% RH, desorption at 60 °C and 30% RH).

During nighttime (Figure 1C), the PV cell is used as an infrared thermal emitter for radiative cooling on the top surface of the hybrid device from the cold universe. The MOF module with packed sorbent captures water vapor from air for driving adsorption to generate adsorption heat. At this time, the hot end (MOF side) and the cold end (PV side) of the TEG module form a temperature difference and generate power through the Seebeck effect. In traditional PV moisture absorption cooling design, the adsorption heat released by adsorbent during the moisture absorption process is dissipated to the environment as waste heat. However, in our hybrid device, the adsorption heat released by the adsorbent is used as the heat source for the hot side of the TEG module, while the coldness obtained from the cosmic radiation cooling is used as the cold source on the cold side of the TEG module. Therefore, the temperature difference between radiative cooling and adsorption heating enables the TEG module to generate electricity at night. It is worthwhile to note that the moisture-sorption heat of the adsorbent increases the hot side temperature of the TEG module, and the heat consumed by the TEG module in turn further accelerates the moisture absorption to capture water vapor from the air by reducing the temperature of the adsorbent. The absorbed water vapor reduces the relative humidity of the outlet, which provides the basis for the application of the hybrid device in the indoor humidity control of the building (Figure 1D).

## Synthesis and characterizations of MOF and PV

The solid dehumidification material has developed rapidly in the past two decades, and in particular, the microporous crystalline materials of metal-organic frameworks (MOFs) have attracted great interest, mainly because they show the advantages of high specific surface area, typical S-shaped isotherms, and good water adsorption properties. So far, many MOFs (MIL-101(Cr)/SA,[39] MOF-303(Al),[40] Al-fumarate/CNTs/SA,[41] etc.) have been studied as water adsorbents for various water collection and moisture absorption device. In this study, we select MIL-101 (Cr) as the solid dehumidification material due to its high-water absorption rate, fast water adsorption kinetics, and adsorption and desorption temperatures suitable for application in outdoor atmospheric environments. Meanwhile, due to the low heat transfer efficiency of MIL-101(Cr), we coat MIL-101(Cr) powders on a copper foam (CF) by the in-situ impregnation method to fabricate MIL-101(Cr)/CF composite as moisture sorbent, and further characterize the morphology and adsorption properties (Figure 2).

SEM and digital photographs image the MIL-101(Cr) particles are regular shaped octahedra with perfect symmetry, and are also uniformly distributed on the porous skeleton of CF (Figure 2A). XRD shows that the synthesized MOF has a good crystal structure, and the $N_2$ adsorption/desorption isotherm images that the surface area of Brunauer-Emmett-Teller (BET) is as high as 2000 $m^2 \cdot g^{-1}$ with an average pore size of 2.38 nm, which provides a good basis for high water adsorption capacity (Figure 2C). The thermal conductivity of adsorbents plays a key role in accelerating heat transfer during moisture adsorption/desorption, but MIL-101(Cr) does not have a good thermal conductivity.[42,43] To overcome the poor heat and mass transfer coefficients of MIL-101(Cr) and accelerate its moisture adsorption/desorption. We selected porous copper foam (CF) with high thermal conductivity and large specific

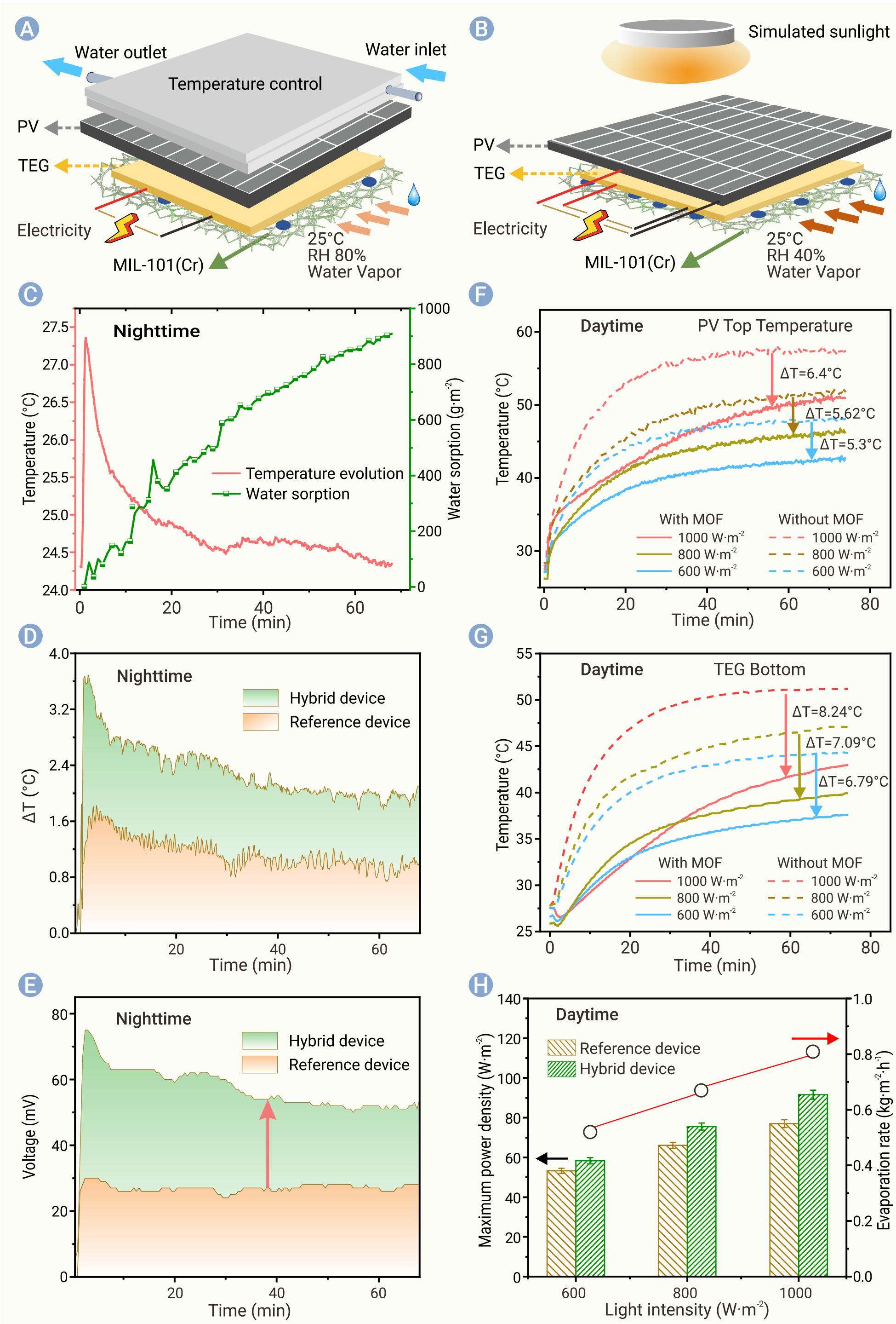


**Figure 3. Proof-of-concept for PV-TEG-MOF hybrid experiments** a Schematic diagram of the hybrid PV-TEG-MOF device using a simulated radiative cooling source at nighttime. b Schematic diagram of moisture desorption and power generation under solar simulator at daytime. c Temperature evolution and water adsorption of hybrid device during moisture sorption process at nighttime. d Temperature difference of the TEG module with and without MOF at nighttime. e Voltage evolution of the TEG module with and without MOF at nighttime. f Temperature evaluations of PV top in the hybrid device with MIL-101(Cr)/CF and the referenced device without MIL-101(Cr)/CF at daytime. g Temperature evaluations of TEG bottom in the hybrid device with MIL-101(Cr)/CF and the referenced device without MIL-101(Cr)/CF at daytime. h Maximum power density and evaporation rate in the hybrid device with MIL-101(Cr)/CF and the referenced device without MIL-101(Cr)/CF at daytime.

surface area as an intermediate to construct the MIL-101(Cr) and CF composite MIL-101(Cr)/CF. Compared with the lower thermal conductivity of MIL-101(Cr) powders (0.15 W·m$^{-1}$·K$^{-1}$), the MIL-101(Cr)/CF exhibits a higher thermal conductivity (1.92 W·m$^{-1}$·K$^{-1}$). The high thermal conductivity and large surface area of the porous copper foam allows for shorter heat transfer paths, which improves the thermal conductivity of MIL-101(Cr)/CF (Figure 2D). These results indicate that the MIL-101(Cr)/CF composites have a porous structure and high thermal conductivity with excellent moisture trapping and heat transport capacity during the moisture absorption/desorption process.

The adsorption experiment was carried out in a constant temperature and humidity chamber, and the experimental data of adsorption were recorded by a high-precision electronic balance (Note S1). The equilibrium capacity of water adsorption for MIL-101(Cr)/CF at constant temperature increased with increasing relative humidity (30, 40, 60 and 80% RH) in the test environment. This phenomenon is consistent with the adsorption properties of adsorbents for water. Theoretically, the increase in relative humidity promotes the collision frequency between adsorbent particles and water molecules, and the adsorbent captures water molecules more easily, thus reaching the adsorption equilibrium state faster. The water adsorption isotherm reveals that MIL-101(Cr)/CF possesses ideal and fast water adsorption properties at 25 °C (Figure 2E & S2). The water adsorption at different temperatures and relative humidities demonstrates its flexible adaptability (Figure 2F), as well as possessed fast water adsorption kinetics (Note S2 & Figure S3). Our results indicated that water uptake and water uptake rate were negatively correlated with working temperature, providing a good basis for the application of materials for nighttime moisture uptake and daytime desorption on buildings. In addition, we have carried out multiple adsorption/desorption cycles on the MIL-101(Cr)/CF composites, and the adsorption capacity is about 0.91g·g$^{-1}$, indicating that the composite exhibits excellent cyclic stability (Figure 2G & S22). MIL-101(Cr)/CF composite has a higher temperature than the ambient temperature during the moisture adsorption process due to a large amount of adsorption heat released by the MOF sorbent (Figure S4).

Benefiting from multiple adsorption isotherms under various temperatures; we calculated isosteric adsorption heat ($\Delta H_s$) from Clausius–Clapeyron equation to estimate the released energy conceived from material-water interaction (Note S2). The isosteric adsorption heat of MIL-101(Cr)/CF is close to the enthalpy of evaporation of water vapor at 25 °C, which is a better candidate for adsorbent adsorption heat to drive TEG for power generation (Figure S5). The good water adsorption capacity of MIL-101(Cr)/CF provides a solid foundation for its use in applications such as heat-driven heat pumps or refrigeration processes.

The earth has a basically transparent atmospheric region in the mid-infrared wavelength range of 8~13μm, which is called the atmospheric window. Through this region, the thermal radiation in the mid-infrared range of the earth is radiated to the cold space at night, resulting in a rapid decline in night temperature. The full-spectrum analyses show that PV has a good absorptivity/emissivity (Figure S6D), thus exhibiting excellent absorption of

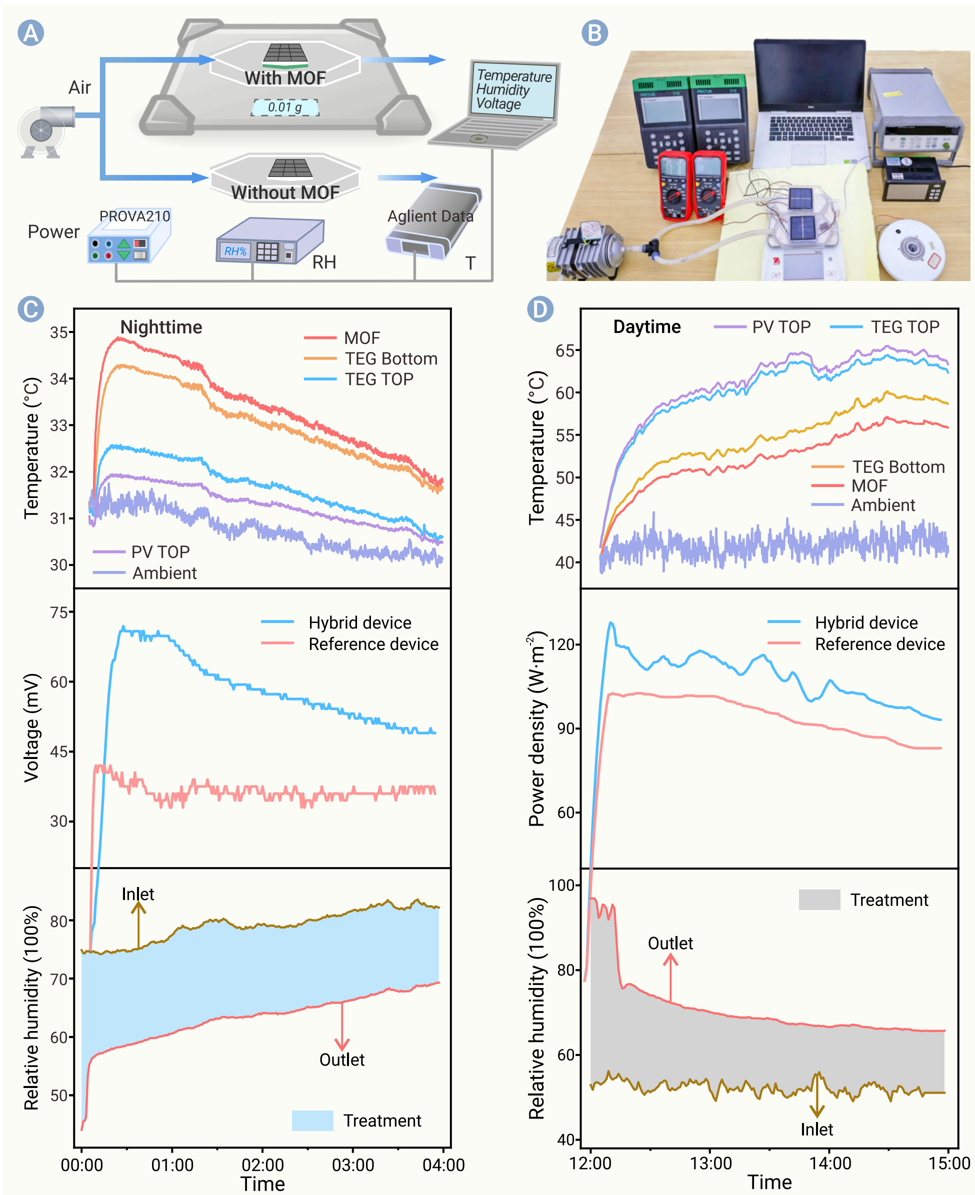


**Figure 4. Outdoor demonstration of the hybrid PV-TEG-MOF device for all-day power generation and humidity control** a Schematic diagram of outdoor experimental setup. b Photograph of outdoor experiment setup. c Real-time evolutions of different temperature, open-circuit voltage, water sorption, and humidity change (air channel) during nighttime. d Real-time evolutions of different temperature, open-circuit voltage, water sorption, and humidity change (air channel) during daytime. d Enthalpy-humidity diagram process of air treatment by air conditioning with and without hybrid device.

solar radiation during the day and good radiative cooling at night. In order to demonstrate the nighttime radiation capacity of PV, we built a self-made experimental test (Note S3). And our results indicate that PV shows good radiation cooling capacity at night. The surface temperature of the test device was a maximum of 7.2 °C lower than the air temperature, and the average surface temperature was reduced by 5.76 °C (Figure S6B). In addition, we calculated the radiant cooling power, which was 40.75 W (Figure S6C). Good radiant cooling capacity provides good applications for the device.

## Proof-of-concept of hybrid PV-TEG-MOF device

We design a hybrid PV-TEG-MOF device for proof-of-concept of all-day energy harvesting in the laboratory (Note S5). The hybrid PV-TEG-MOF device is assembled by a PV module, TEG module, and MOF module (Figure 3). To verify that adsorption heat synergistically promotes TEG power generation, we specially designed a referenced device without MIL-101(Cr)/CF compared to the hybrid PV-TEG-MOF device with MIL-101(Cr)/CF. Meanwhile, in the nighttime radiative cooling experiments, the photovoltaic surface temperature was reduced by an average of 5.76 °C compared to the outdoor ambient temperature. Therefore, we used a water-cooling radiator with 5 °C lower than the ambient temperature to simulate the radiative cooling effect in the laboratory by referring to the reported results.[44,45] Areal power density ($P_{density}$) was calculated by the equation:

$$P_{density} = V_{oc}^{2}/(4 \times R_{module} \times A_{module})$$

where $V_{oc}$, $R_{module}$, and $A_{module}$ were the measured open-circuit voltage, resistance, and the area of TEG module, respectively.

To evaluate the performance of the hybrid device under simulated conditions at nighttime, we extracted air from a constant temperature and humidity test chamber into the PV-TEG-MOF device, and controlled the adsorption experimental conditions of 80% RH and 25°C for moisture adsorption and power generation (Figure S7). The MIL-101(Cr)/CF composite module captures water vapor from the air, and its mass gradually increased during the moisture adsorption process (Figure 3C). The adsorption heat released by MIL-101(Cr) increases the temperature of the MIL-101(Cr)/CF, and the excess heat is dissipated to the environment, resulting in a slightly higher outlet temperature than the inlet temperature, and then stabilizes as the adsorption process proceeds (Figure S8). The hybrid device achieved the highest temperature difference (ΔT=3.6 °C) by combining adsorption heating and radiative cooling compared to the reference device (Figure 3D). The maximum voltages of the TEG module are 75 and 30 mV, respectively, for the devices based on MIL-101(Cr)/CF and without MIL-101(Cr)/CF (Figure 3E); and the corresponding average $P_{density}$ are 93.31 and 20.57 mW·m$^{-2}$ (Figure S9). Therefore, the synergistic effect of adsorption heating and radiation cooling in the hybrid PV-TEG-MOF device improve the thermoelectric power density by 353% compared to without MIL-101(Cr)/CF design.

To evaluate the performance of the hybrid device under simulated conditions at daytime, we conducted indoor experiments using solar simulators with different sunlight intensities (Figure S10). The moisture desorption conditions were controlled at 40% RH and 25 °C. The solar simulator provides energy to the PV module, and drives the moisture desorption to promote thermoelectric power generation (Figure 3B). The hybrid PV-TEG-MOF device and the reference device without MIL-101(Cr)/CF have similar temperature evolutions under different simulated solar intensities, and the temperature at the TEG bottom increases with the increase of sunlight (Figure 3G), indicating that the waste heat generated by the PV can be efficiently transferred to the MIL-101(Cr)/CF. However, MIL-101(Cr)/CF exhibits a pronounced capacity for absorption heat during moisture desorption, resulting in a reduction in temperature at the base of the TEG within the hybrid device relative to the reference device (Figure 3F & S11). For instance, under one standard sun (1000 W·m$^{-2}$), the maximum TEG bottom temperature of the hybrid PV-TEG-MOF device with MIL-101(Cr)/CF is 43.25 °C, ~8.24 °C lower than that of the reference device without MIL-101(Cr)/CF; and the PV TOP temperature is 57.34°C, compared to the reference device temperature is 6.4°C lower (Figure 3G). The results demonstrate that MOF module can effectively cool the PV during moisture desorption, and increase the service life of the PV modules

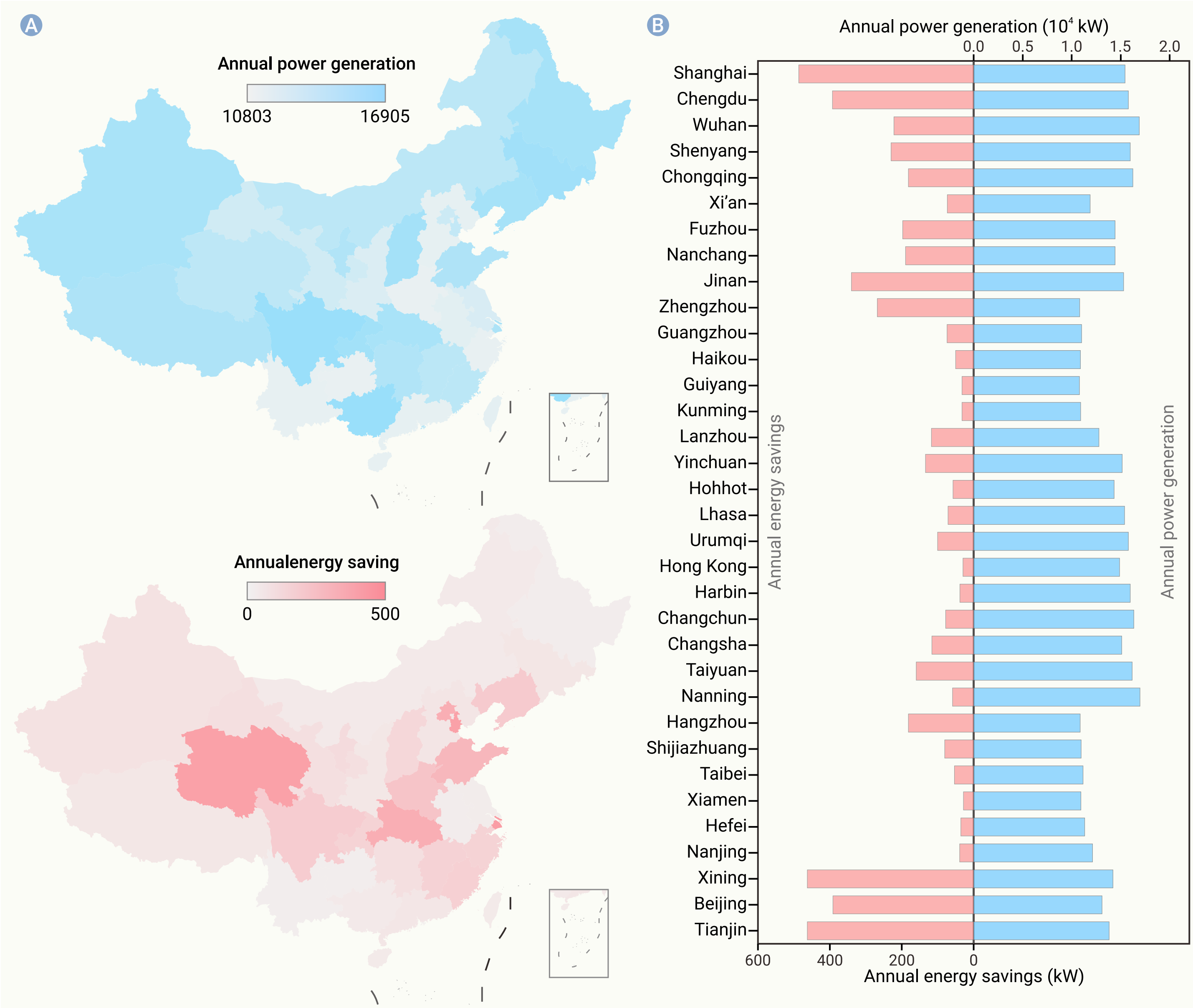


**Figure 5. Dehumidification and power generation of multi-functional roof modeling analysis** a Application performance for different cities in China. b Annual power generation and average annual energy savings in different cities

while improving their efficiency. Therefore, the desorption heat of the hybrid device improves the thermoelectric power generation and enhances the PV efficiency by providing a good cooling effect.

The hybrid and reference devices have similar evolutions of TEG open-circuit voltage (TEG) and the power density (PV) at different simulated sunlight intensities. High sunlight intensity provides more energy to the PV module, and thus generates more waste heat to increase the thermoelectric power density. As a result, the power density (PV) and the maximum $V_{oc}$ (TEG) increase with increasing sunlight intensity. For example, at solar fluxes of 600, 800, and 1000 W·m$^{-2}$, the maximum $V_{oc}$ (TEG) of the hybrid device was 159.6, 205.1, and 257.3 mV (Figure S12), the average power density (TEG) was 290.75, 472.1, and 757.8 mW·m$^{-2}$ (Figure S13). Furthermore, the hybrid device has a higher performance than the reference device for a given sunlight intensity. In addition, we calculated the overall power density of the device ($P_{device}$) (Figure 3H). More specifically, under a standard sun (1000 W·m$^{-2}$), the maximum $V_{oc}$ of the TEG using MIL-101(Cr)/CF is improved from 220 to 403 mV; the maximum power of the PV module rises from 77.2 to 93.6 W·m$^{-2}$; the average $P_{device}$ rises from 75.63 to 91.03 W·m$^{-2}$. These results demonstrate that the PV-TEG-MOF hybrid device has excellent power generation performance, and the average power density of the hybrid device is increased by 20.3% compared with the reference PV-TEG device. This is because the MOF material needs to absorb heat for desorption during the day. The heat generated by photovoltaics is utilized by the MOF material to increase the power of the hybrid device.

## Outdoor demonstration of all-day power generation and humidity control

In order to evaluate the outdoor dehumidification and power generation potential of the hybrid PV-TEG-MOF device, we further conducted outdoor experiments on the roof of the Tiangong Building in Nanjing Tech University, China. The hybrid PV-TEG-MOF device is shown below and the reference device without MIL-101(Cr)/CF is shown above (Figure 4B). At nighttime, the hybrid PV-TEG-MOF device captures moisture from the air and generates electricity through adsorptive heating of MIL-101(Cr)/CF during the moisture absorption process in conjunction with cold cosmic radiation cooling from cold universe. At the same time, the MIL-101(Cr)/CF moisture absorption process reduces the air relative humidity, thus providing comfortably dry air. During the daytime, the hybrid device generates electricity from PV-TEG by synergistic collection of radiation heat from sunlight and desorption cooling from moisture desorption.

We performed the power generation and humidity testing of both systems

Table 1. Average power generation and energy savings by climate zone and deployment recommendations.

| Climate Zone | Typical Cities | Characteristics | Avg. PV Generation (kW) | Avg. AC Energy Savings (kW) | Deployment Recommendation |
|---|---|---|---|---|---|
| Cold Regions | Beijing; Shenyang, etc. | Significant humidity fluctuations (RH 40-75%) in transitional seasons | $1.34 \times 10^4$ | 255.28 (Highest) | Priority Deployment |
| Temperate Regions | Kunming; Dali, etc. | Annual temperature 15-20°C, RH 55-65%; >40% cloudy days | $1.31 \times 10^4$ | 53.1 (Lowest) | Defer Deployment |
| Hot Summer/Cold Winter Regions | Shanghai; Wuhan, etc. | Hot-humid summers, chilly-damp winters; 40-60-day plum rain season | $1.39 \times 10^4$ | 192.39 | Priority Deployment |
| Hot Summer/Warm Winter Regions | Guangzhou; Shenzhen, etc. | Year-round high temperatures; High-humidity rainy seasons | $1.28 \times 10^4$ (Lowest) | 71.92 | Selective Deployment |
| Severe Cold Regions | Harbin, Wulumuqi, etc. | Prolonged winter (>6 months) with extremes; Higher humidity in winter and lower humidity in summer | $1.56 \times 10^4$ (Highest) | 103.15 | Selective Deployment |

on July 25th 00:00 am to 4:00 am. Temperature, humidity and open circuit voltage were measured during this period (Figure 4C). The top temperature of a conventional radiatively cooled power generation device will be a lower than the ambient outdoor temperature due to radiative cooling.[46] In this study, the PV top temperature of this hybrid PV-TEG-MOF device is higher than the ambient temperature, although the top of the hybrid device is also cooled by radiative cooling (Figure 4C). These results indicate that the adsorption heat of the MIL-101(Cr)/CF is higher than the radiative cooling of the universe. In addition, our results indicated that the hybrid device has a larger open-circuit voltage and $\Delta T_{TEG}$ (Maximum $\Delta T_{TEG}$ is 4.3 °C) compared to the reference device, because the adsorption heat further widens the TEG temperature difference (Figure S14). We calculated the maximum power densities of the hybrid and reference devices to be 114.7 and 40.3 $mW \cdot m^{-2}$, respectively. Meanwhile, we further analyzed the power of the hybrid and reference devices, and the average power density was increased by 152% (Figure S15).

In addition, indoor relative humidity affects thermal comfort. The American Society of Heating, Refrigerating, and Air-Conditioning Engineers (ASHRAE) recommends an appropriate livable indoor RH in the range of 40% to 65%. In this study, it was indicated that the MOF absorbed 0.7 $g \cdot g^{-1}$ of water within 4 hours at an average relative humidity of 79.12% ambient conditions. The average RH of the output air is at 63.34%, which is 15.78% lower than the ambient relative humidity. At the same time, the inlet and outlet average temperature of the device is 31.1 °C and 33.5 °C, and the outlet temperature has a small range of temperature rise (Figure S16). In order to evaluate the impact of the temperature rise and relative humidity drop brought about by the outlet of the device on the energy consumption of the indoor environment, we analyzed it using the energy demand of the air conditioning system (Note S4, Figure S17). Without hybrid device, the total air conditioning energy demand is 55.1 W for RH of 79.12 and temperature of 31°C. The total air conditioning energy demand for the system using the PV-TEG-MOF device is 37.8 W, which is a 43.6% reduction in energy demand compared to the system without the hybrid device. If the hybrid device is applied to the building, it can treat indoor air with high humidity to a comfortable range for human, while replacing the dehumidifying function of air conditioners to reduce the building energy consumption.

During the daytime, the hybrid PV-TEG-MOF device achieves power generation by synergistically harvesting radiant heat from the sun and cooling with moisture desorption (Figure 4B). The test was taken place on July 26th from 12:00 to 15:00 pm. The hybrid device was sealed after outdoor nighttime experiments and then opened for moisture desorption and water collection during daytime experiments. The PV module converts the energy from solar radiation into electrical energy while the waste heat generated feeds the lower TEG. In addition, adsorbent desorption leads to a decrease in the MIL-101(Cr)/CF temperature, but the overall temperature still shows an increase due to solar radiation (Figure S18). The relative humidity was initially large due to sealing and decreased significantly after air was introduced. This is because the evaporation of water vapor stored in the adsorbent at night causes the relative humidity at the outlet to increase. The MOF material has a cooling effect on the PV, resulting in a higher power density of the hybrid device than the reference device. The average output power density of the reference device is 86.7 $W \cdot m^{-2}$ and the average output power density of the hybrid device is 100.65 $W \cdot m^{-2}$, which is 13.95 $W \cdot m^{-2}$ higher than the reference device (Figure 4D).

Furthermore, we carried out continuous five-day outdoor experiment to demonstrate simultaneous dehumidification and all-day power generation (Figure S19). The daytime tests were conducted from 12:00 to 15:00 pm, and the nighttime tests were conducted from 00:00 to 4:00 am. The hybrid PV-TEG-MOF device has a continuous voltage output, with a maximum open-circuit voltage of 283 mV, and the power output of the hybrid device is excellent, with an average daytime power density of 83 $W \cdot m^{-2}$. Notably, the data showed that the outlet relative humidity of the hybrid device is stable between 50% and 65%, indicating that the treated air maintains a good and stable humidity buffer range.

## Integrated simulation analysis of composite device building roofs

We propose an interesting component combining solid dehumidification materials and photovoltaics, a hybrid device that effectively improves the co-generation capacity of PV-TEG and shows excellent performance in humidity regulation. It can be widely used in building components such as Trombe walls and roofs, providing a good balance between building energy consumption and indoor air quality. As shown in Figure S24, it actively reduces indoor humidity levels by adsorbing water vapor during high humidity conditions at night, and then releasing the water vapor during the daytime in hot environments. This adsorption-desorption function successfully controls humidity and creates a comfortable living environment. At the same time, the electricity generated by the PV can be applied to indoor appliances, such as refrigerators and lighting, reducing the building's energy consumption. In order to explore the practical architectural applications of the device, we built a roof model using Matlab to evaluate the potential of multifunctional roof for power generation and dehumidification performance. The model dimensions of the hybrid device on the roof measure 5 m in both length and width. We simulate the power generation and energy savings after installing PV-TEG-MOF hybrid device on the roofs in different cities to examine its applicability (Figure 5A).

The simulation of system performance was conducted in Nanjing for three days to demonstrate the potential of the hybrid device for architectural applications. Under the favorable outdoor temperature and solar radiation conditions, the multi-functional roof had continuous power output during the day and night. For example, the predicted maximum power obtained during the day being 2.2 kW and the predicted maximum power obtained during the night being 53 W in Nanjing. Compared with the relative humidity before treatment, the use of this roof saves 0.11 kW of air conditioning energy consumption in Nanjing (Figure S20). At the same time, the performance of a hybrid roof can be affected by the weather conditions. We analyzed the performance for favorable and unfavorable weather conditions (sunny and cloudy day) in Nanjing. Our results indicated that the multifunctional roof system exhibited excellent power generation and dehumidification performance on sunny days, but on cloudy day the system power output drops by 60.7% and dehumidification performance drops by 64.95% (Figure S23). In order to cope with this degradation of performance on cloudy days, we suggest that the system can be integrated with an electric auxiliary heat module to enhance MOF desorption capacity under cloudy conditions.

Moreover, we also calculated typical annual power generation and air conditioning energy savings for 34 cities in China. The multi-functional roof has shown good annual power generation and annual energy savings performance in different cities in China, generating more than $1.08\times10^4$ kW in different cities, with a maximum of $1.69\times10^4$ kW in Wuhan, and the annual energy savings in air-conditioning ranges from 29 kW to 498 kW in different cities (Figure 5B). Further, the application performance of hybrid roofs was analyzed by climate zone, as shown in Table 1. The system achieved the highest power output ($1.56\times10^4$ kW) through MOF module-enhanced dehumidification during high-humidity transitional seasons in severe cold regions, while system showed minimal energy-saving benefits (53.1 kW) in temperate zones due to environmentally suitable humidity levels. Deployment prioritization should focus on hot summer/cold winter and cold climate zones where humidity load characteristics synergistically improve both power efficiency and dehumidification return, with temperate regions temporarily excluded from implementation due to their naturally habitable thermal-humidity conditions yielding unfavorable cost-benefit ratios for MOF module applications.

Economic performance analysis plays a critical role in evaluating technological viability and adoption potential. We conducted a systematic comparison between commercial dehumidifiers and our proposed MOF-based dehumidification system. While the system exhibits higher costs and lower daily dehumidification capacity compared to traditional systems, which enables significant reductions in long-term energy consumption and electricity expenditures (Table S2). At the same time, we conducted a cost analysis for a 5m×5m residential building in Nanjing. The system demonstrates an initial investment of ¥11148, annual revenue of ¥7420.33, and a payback period of 1.5 years (Note S7). The economics of this system in Nanjing were systematically evaluated through a life-cycle cost analysis, which showed that the system has good potential for return on investment.

## DISCUSSION

In this paper, we propose an innovative strategy for simultaneous dehumidification and all-day power generation by subtly harnessing the effects of moisture adsorption/desorption, solar radiation heating, and radiative cooling from the universe in a PV-TEG device in combination with a solid dehumidification material (MIL-101(Cr)). The outdoor nighttime experiments demonstrate that the hybrid device has 152% higher average power density than the reference device and the average RH of the output air is at 68.01%, which is 11.11% lower than the ambient relative humidity. During outdoor daytime experiments, the hybrid device achieved an average power density of 100.65 $W{\cdot}m^{-2}$, outperforming the reference device by 13.95 $W{\cdot}m^{-2}$.

Simulations of the device applied to a building roof in Nanjing predicted a continuous power output, with a predicted maximum power of 2.2 kW during the day and 53 W in during the night. Additionally, the treated air maintained relative humidity level between 47% to 58%, which is in line with the optimal residential humidity range for Nanjing. The multi-functional roof demonstrated excellent performance across various cities in China, generating more than $1.08\times10^4$ kW, with a peak of $1.69\times10^4$ kW in Wuhan. Meanwhile, the multi-functional roof showed robust dehumidification capabilities in cities such as Nanchang, Jinan and Zhengzhou. Our study provides a viable strategy for integrating PV-TEG-MOF systems with buildings to achieve both continuous power generation and indoor humidity control in buildings.

## REFERENCES


1. Ballif C., Perret-Aebi L. E., Lufkin S., et al. (2018). Integrated thinking for photovoltaics in buildings. *Nat. Energy.* 3:438–442. DOI:10.1038/s41560-018-0176-2
2. González-Torres M., Pérez-Lombard L., Coronel J. F., et al. (2022). A review on buildings energy information: Trends, end-uses, fuels and drivers. *Energy. Rep.* 8:626–637. DOI:10.1016/j.egyr.2021.11.280
3. Heer P., Derungs C., Huber B., et al. (2024). Comprehensive energy demand and usage data for building automation. *Sci. Data.* 11. DOI:10.1038/s41597-024-03292-2
4. Jani D. B., Mishra M. and Sahoo P. K. (2016). Solid desiccant air conditioning - A state of the art review. *Renew. Sust. Energ. Rev.* 60:1451–1469. DOI:10.1016/j.rser.2016.03.031
5. Li X. Y., Zhao Q. Q. and Qu D. Q. (2015). Investigation on the dynamic characteristics of a direct contact thermal energy storage charging process for use in conventional air-conditioning systems. *Appl. Therm. Eng.* 91:172–180. DOI:10.1016/j.applthermaleng.2015.08.005
6. Harriman L. G., Plager D. and Kosar D. (1997). Dehumidification and cooling loads from ventilation air. *Ashrae. J.* 39:37. DOI:10.1080/01998595.1999.10530479
7. Castellano J., Sanz V., Cañas E., et al. (2022). Assessment of humidity self-regulation functionality for ceramic tiles. *J. Eur. Ceram. Soc.* 42:716–723. DOI:10.1016/j.jeurceramsoc.2021.10.025
8. Castellano J., Sanz V., Cañas E., et al. Assessment of humidity self-regulation functionality for ceramic tiles. *J. Eur. Ceram. Soc.* Li M., Nicolas V., Khelifa M., et al. (2019). Modelling the hygrothermal behaviour of cement-bonded wood composite panels as permanent formwork. *Ind. Crop. Prod.* 142. DOI:10.1016/j.indcrop.2019.111784
9. Castellano J., Sanz V., Cañas E., et al. Assessment of humidity self-regulation functionality for ceramic tiles. *J. Eur. Ceram. Soc.* Qin M. G., Hou P. M., Wu Z. M., et al. (2020). Precise humidity control materials for autonomous regulation of indoor moisture. *Build. Environ.* 169. DOI:10.1016/j.buildenv.2019.106581
10. Ybyraiymkul D., Chen Q., Burhan M., et al. (2023). Innovative solid desiccant dehumidification using distributed microwaves. *Sci. Rep. Uk.* 13. DOI:10.1038/s41598-023-34542-9
11. Ge L. R., Feng Y. H., Wu J. R., et al. (2024). Performance evaluation of MIL-101(Cr) based desiccant-coated heat exchangers for efficient dehumidification. *Energy* 289. DOI:10.1016/j.energy.2023.130049
12. Cao B. Y., Tu Y. D. and Wang R. Z. (2019). A Moisture-Penetrating Humidity Pump Directly Powered by One-Sun Illumination. *Iscience* 15:502. DOI:10.1016/j.isci.2019.05.013
13. Yan J., Yu Y., Ma C., et al. (2015). Adsorption isotherms and kinetics of water vapor on novel adsorbents MIL-101(Cr)@GO with super-high capacity. *Appl. Therm. Eng.* 84:118–125. DOI:10.1016/j.applthermaleng.2015.03.040
14. Hashjin M. A., Zarshad S., Emrooz H. B. M., et al. (2023). Enhanced atmospheric water harvesting efficiency through green-synthesized MOF-801: a comparative study with solvothermal synthesis. *Sci. Rep. Uk.* 13. DOI:10.1038/s41598-023-44367-1
15. He Y., Fu T., Wang L. J., et al. (2023). Self-assembly of MOF-801 into robust hierarchically porous monoliths for scale-up atmospheric water harvesting. *Chem. Eng. J.* 472. DOI:10.1016/j.cej.2023.144786
16. Cui S. Q., Qin M. H., Marandi A., et al. (2018). Metal-Organic Frameworks as advanced moisture sorbents for energy-efficient high temperature cooling. *Sci. Rep. Uk.* 8. DOI:10.1038/s41598-018-33704-4
17. Nayak P. K., Mahesh S., Snaith H. J., et al. (2019). Photovoltaic solar cell technologies: analysing the state of the art. *Nat. Rev. Mater.* 4:269–285. DOI:10.1038/s41578-019-0097-0
18. Hayat M. B., Ali D., Monyake K. C., et al. (2019). Solar energy-A look into power generation, challenges, and a solar-powered future. *Int. J. Energ Res.* 43:1049–1067. DOI:10.1002/er.4252
19. Huang J. C., Chen X., Yang H. X., et al. (2018). Numerical investigation of a novel vacuum photovoltaic curtain wall and integrated optimization of photovoltaic envelope systems. *Appl. Energy* 229:1048–1060. DOI:10.1016/j.apenergy.2018.08.095
20. Tang Y. Y., Ji J., Zhang C. Y., et al. (2024). An advanced exhausting airflow photovoltaic curtain wall system coupled with an air source heat pump for outdoor air treatment: Energy-saving performance assessment. *Energy Convers. Manag.* 299. DOI:10.1016/j.enconman.2023.117872
21. Tan Y. T., Peng J. Q., Luo Z. Y., et al. (2023). Multi-function partitioned design method for photovoltaic curtain wall integrated with vacuum glazing towards zero-energy buildings. *Renew. Energ.* 218. DOI:10.1016/j.renene.2023.119257
22. Meng Y., Tan Y. T., Li X., et al. (2022). Building-integrated photovoltaic smart window with energy generation and conservation. *Appl. Energy* 324. DOI:10.1016/j.apenergy.2022.119676
23. Bing J. M., McKenzie D. R., Stals T., et al. (2023). Perspective Total equivalent energy efficiency metric for building-integrated photovoltaic windows. *Joule* 7:2668–2683. DOI:10.1016/j.joule.2023.11.010
24. Liu H. X., He W., Liu X. H., et al. (2023). Building integrated concentrating photovoltaic window coupling luminescent solar concentrator and thermotropic material. *Energy* 284. DOI:10.1016/j.energy.2023.129237
25. Joshi S., Mittal S., Holloway P., et al. (2021). High resolution global spatiotemporal assessment of rooftop solar photovoltaics potential for renewable electricity generation. *Nat. Commun.* 12. DOI:10.1038/s41467-021-25720-2
26. Chen T. Y., Zhang N., Ye Z. B., et al. (2024). Carbon reduction benefits of photovoltaic-green roofs and their climate change mitigation potential: A case study of Xiamen city. *Sustain. Cities Soc.* 114. DOI:10.1016/j.scs.2024.105760
27. Ma Q. L., Zhang Y., Wu G., et al. (2022). Photovoltaic/spectrum performance analysis of a multifunctional solid spectral splitting covering for passive solar greenhouse roof. *Energy Convers. Manag.* 251. DOI:10.1016/j.enconman.2021.114955

28. Zhang Z. X., Chen M., Zhong T., et al. (2023). Carbon mitigation potential afforded by rooftop photovoltaic in China. *Nat. Commun.* 14. DOI:10.1038/s41467-023-38079-3
29. Libra M., Petrik T., Poulek V., et al. (2021). Changes in the Efficiency of Photovoltaic Energy Conversion in Temperature Range With Extreme Limits. *Ieee J Photovolt* 11:1479–1484. DOI:10.1109/Jphotov.2021.3108484
30. Huang G., Xu J. Y. and Markides C. N. (2023). High-efficiency bio-inspired hybrid multi-generation photovoltaic leaf. *Nat. Commun.* 14. DOI:10.1038/s41467-023-38984-7
31. Liu J. W., Zhou Y. F., Zhou Z. H., et al. (2024). Passive Photovoltaic Cooling: Advances Toward Low-Temperature Operation. *Adv. Energy Mater.* 14. DOI:10.1002/aenm.202302662
32. Bamisile O., Acen C., Cai D. S., et al. (2025). The environmental factors affecting solar photovoltaic output. *Renew. Sust. Energy Rev.* 208. DOI:10.1016/j.rser.2024.115073
33. Khan M. A. I., Khan M. I., Kazim A. H., et al. (2021). An Experimental and Comparative Performance Evaluation of a Hybrid Photovoltaic-Thermoelectric System. *Front. Energy Res.* 9. DOI:10.3389/fenrg.2021.722514
34. Yang B., Wu S. C., Huang J. X., et al. (2023). Salp swarm optimization algorithm based MPPT design for PV-TEG hybrid system under partial shading conditions. *Energy Convers. Manag.* 292. DOI:10.1016/j.enconman.2023.117410
35. Xu L., Luo K., Ji J., et al. (2020). Study of a hybrid BIPV/T solar wall system. *Energy* 193:116578. DOI:https://doi.org/10.1016/j.energy.2019.116578
36. Yu B. D., Li N. S., Yan C. C., et al. (2022). The comprehensive performance analysis on a novel high-performance air-purification-sterilization type PV-Trombe wall. *Renew. Energ.* 182:1201–1218. DOI:10.1016/j.renene.2021.11.029
37. Yang M., Zhong H. M., Li T., et al. (2023). Phase Change Material Enhanced Radiative Cooler for Temperature-Adaptive Thermal Regulation. *Acs. Nano.* 17:1693–1700. DOI:10.1021/acsnano.2c11916
38. Ding T. P., Zhu L. L., Wang X. Q., et al. (2018). Hybrid Photothermal Pyroelectric and Thermogalvanic Generator for Multisituation Low Grade Heat Harvesting. *Adv. Energy Mater.* 8. DOI:10.1002/aenm.201802397
39. Tao Y. L., Li Q. Q., Wu Q. N., et al. (2021). Embedding metal foam into metal-organic framework monoliths for triggering a highly efficient release of adsorbed atmospheric water by localized eddy current heating. *Mater. Horiz.* 8:1439–1445. DOI:10.1039/d1mh00306b
40. Hanikel N., Prévot M. S., Fathieh F., et al. (2019). Rapid Cycling and Exceptional Yield in a Metal-Organic Framework Water Harvester. *Acs. Central Sci.* 5:1699–1706. DOI:10.1021/acscentsci.9b00745
41. Tao Y. L., Wu Q. N., Huang C., et al. (2022). Sandwich-Structured Carbon Paper/Metal-Organic Framework Monoliths for Flexible Solar-Powered Atmospheric Water Harvesting On Demand. *Acs. Appl. Mater. Inter.* 14:10966–10975. DOI:10.1021/acsami.1c23644
42. Jiménez-Laines G., Flores E., García-Peña N. G., et al. (2023). Double step heating synthesis of MIL-101(Cr) composites for water harvesting applications. *Micropor Mesopor. Mat.* 362. DOI:10.1016/j.micromeso.2023.112782
43. Permyakova A., Wang S. J., Courbon E., et al. (2017). Design of salt-metal organic framework composites for seasonal heat storage applications. *J. Mater. Chem. A* 5:12889–12898. DOI:10.1039/c7ta03069j
44. Fan S. H. and Raman A. (2018). Metamaterials for radiative sky cooling. *Nat. Sci. Rev.* 5:132–133. DOI:10.1093/nsr/nwy012
45. Raman A. P., Li W. and Fan S. H. (2019). Generating Light from Darkness. *Joule* 3:2679–2686. DOI:10.1016/j.joule.2019.08.009
46. Hossain M. M. and Gu M. (2016). Radiative Cooling: Principles, Progress, and Potentials. *Adv Sci* 3. DOI:10.1002/advs.201500360



## FUNDING AND ACKNOWLEDGMENTS

The funders had no role in study design, data collection and analysis, decision to publish, or preparation of the manuscript. This research is supported by the National Natural Science Foundation of China (No. 52238004 and No. 52278111), Natural Science Foundation of Jiangsu Province (No. BK20221315), Youth Science and Technology Talent Support Project of Jiangsu Province (No. JSTJ-2024-190), Engineering and Physical Sciences Research Council for funding support to the Marie Sklodowska-Curie fellowship (Horizon Europe Guarantee grant number: EP/Y016645/1).


## DECLARATION OF INTERESTS

The authors declare that they have no known competing financial interests or personal relationships that could have appeared to influence the work reported in this paper.

## DATA AND MATERIALS AVAILABILITY

Requests for further information and resources should be directed to and will be fulfilled by the lead contact.

## SUPPLEMENTAL INFORMATION

Supplemental information includes seven notes, twenty-four figures and two tables. It can be found at: https://doi.org/10.59717/j.xinn-energy.2025.100078

## LEAD CONTACT WEBSITE

Bendong Yu: https://www.x-mol.com/groups/Yu_Bendong123/people/53264